Chemical Engineering & Processing: Process Intensification 143 (2019) 107599

Contents lists available at ScienceDirect

Chemical Engineering & Processing: Process Intensification

journal homepage: www.elsevier.com/locate/cep

Prediction of critical mass rate of flashing carbon dioxide flow in convergent-divergent nozzle

Wojciech Angielczyk[a], Jean Marie Seynhaeve[b], Jerzy Gagan[a], Yann Bartosiewicz[b], Dariusz Butrymowicz[a,*]

[a] Bialystok University of Technology, Wiejska 45C, Bialystok, 15-351, Poland
[b] Université catholique de Louvain UCL (iMMC), Belgium

ARTICLE INFO

Keywords:
Nozzle
Two-phase flow
Critical mass flow rate
Transonic trajectory determination
Ejector

ABSTRACT

The prediction of a critical mass flow rate of flashing flow is of crucial importance for many applications in chemical and processing apparatus. One of the most prosperous application is the two-phase ejector as a device with flashing liquid phase as a motive fluid and vapour phase as a secondary fluid. In that case the prediction of critical flashing flow mass flow rate is necessary. A new generalised procedure of the transonic trajectory determination that uses enhanced Possible-Impossible Flow algorithm is proposed. The procedure is much faster than the commonly used Newton Critical Point (NCP) approach. The approach was applied in modelling of carbon dioxide transonic two-phase flow through the convergent-divergent nozzle by means of Homogeneous Equilibrium Model (HEM) and Delayed Equilibrium Model (DEM). These models were used to simulate flows that were experimentally and theoretically investigated in literature. The application of DEM model for determination of the supersonic trajectory part for CO_2 flow is a novel contribution provided in the paper. The comparison with literature experimental data revealed that the original closure equations developed for water are improper for CO_2 transonic flows, thus the adjusting attempts were demonstrated. It was revealed that the applied Darcy friction factor determination approach significantly influences on the results. Moreover, an effective DEM adjustment is impossible until Lockhart–Martinelli approach is utilised. It was shown that for CO_2 case Darcy friction factor calculated by means of Friedel approach is more appropriate than the one calculated by means of the commonly used Lockhart–Martinelli approach. Nevertheless, it was demonstrated that using a frictionless approach would still give better results while adjusting DEM to better approximate the experimental pressure distributions.

1. Introduction

The prediction of a critical mass flow rate is of crucial importance for an appropriate design of most of apparatus applied in chemical and process engineering. Special attention should be paid to various types of the ejector systems applied in processing and reactor engineering with liquid applied as a motive fluid, Pangarkar [1] Weber et al. [2] Rahman et al. [3] Gamisans et al. [4]. Depending on the operation conditions, flashing process can occur in the liquid motive nozzle so that the correct prediction of mass flow rate may be thought as necessary to design this apparatus. The ejectors and flashing process may be also applied in cooling devices of various types, e.g. Abed et al. [5] Haida et al. [6].

The schematic of a two-phase ejector with subcooled liquid phase as a motive fluid and vapour phase as a secondary fluid is presented in Fig. 1a. The liquid phase due to depressurisation achieves saturation conditions and partly evaporates inside the nozzle so that two-phase flow emanates from the nozzle. Due to momentum transfer between a motive jet and vapour, the vapour is entrained into the suction chamber and then flows into the mixing chamber. Further, as an effect of the momentum transfer, mixing process occurs along with formation of a two-phase shock wave with rise of static pressure. Then the mixed homogeneous two-phase flow is additionally compressed in the diffuser achieving the discharge pressure p_m.

The subcooled liquid enters the motive nozzle and partly evaporates inside due to depressurisation, see Fig. 1b. The flashing process is characterised by high thermal non-equilibrium (i.e. temperature difference across the interface): despite that at a certain location, the equilibrium saturation pressure is achieved, the nucleation process does not start and a metastable liquid flow occurs up to a location where the metastable liquid is sufficiently superheated to sustain the vapour

* Corresponding author.
E-mail address: d.butrymowicz@pb.edu.pl (D. Butrymowicz).

https://doi.org/10.1016/j.cep.2019.107599
Received 22 February 2019; Received in revised form 8 July 2019; Accepted 9 July 2019
Available online 23 July 2019
0255-2701/

Nomenclature

A	flow channel cross, m^2
A_{ij}	coefficient matrix of eq. system (10)
b_j	source terms vector of eq. system (10)
C	channel perimeter, m
C_1	C_2, C_3,constants in eq. (9)
D	determinant of matrix A_{ij}
h	specific enthalpy, J kg^{-1}
m	mass flow rate, kg s^{-1}
N_i	i-th determinant of eq. system (10)
n	number of equations/(independent variables) in eq. system (10)
p	pressure, Pa
q	heat flux, W m^{-2}
T	temperature, °C
t	dummy parameter in eq. system (11)
v	specific volume, m^3 kg^{-1}
w	velocity, m s^{-1}
x	quality/vapor mass fraction
y	vaporization index
z	coordinate in flow direction, m

Greek symbols

α	nozzle divergent part angle, rad
Δ	used before a quantity symbol denotes a change in the quantity
δ	discrepancy between experimental and calculated pressure, $\delta = p_{exp} - p_{calc}$, *MPa*
δ_r	relative discrepancy between experimental and calculated pressure, $\delta_r = 100\ \delta/p_{exp}$
ρ	density, kg m^{-3}
σ	velocity-state vector in eq. (10)
τ	wall shear stress, Pa

subscripts

c	fluid critical point
ml	metastable fraction
in	inlet
s	saturated
sg	saturated vapour
sl	saturated liquid

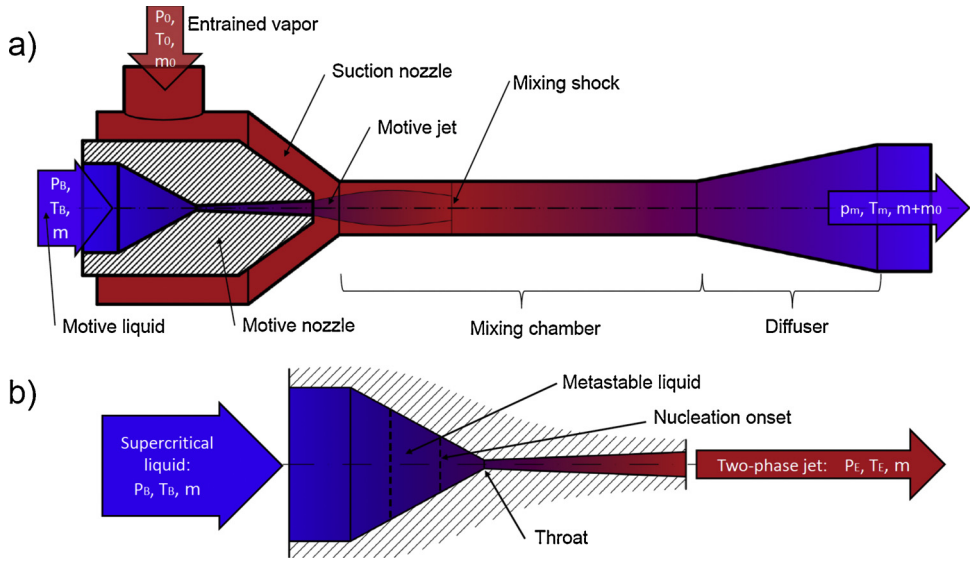

Fig. 1. Physical situation: a) two-phase ejector; b) flashing process in the converging-diverging nozzle.

nucleation, as it was explained by Attou et al. [7]. From that location, the two-phase flashing flow is formed. In this case, the vapour phase growth rate is limited by the interphase heat transfer rate rather instead of mechanical expansion. However, under real operation conditions, both mechanical and thermal non-equilibrium exist simultaneously during flashing process making strong difficulties to accurately predict critical mass flow rate through the motive nozzle.

Although numerical modelling with CFD was applied recently to predict critical mass flow rate through the converging-diverging motive nozzles, e.g. Janet et al. [8], the non-equilibrium effects require further studies in possible application of available modelling approaches of two-phase critical flows. One dimensional modelling is less time-consuming than CFD modelling. Moreover, it is much easier to recognise and interpret physical processes in one dimensional approach, thus this approach may be thought as the most suitable for the considered study. Due to recent applications of two-phase ejectors in refrigeration systems, e.g. Palacz et al. [9] Smolka et al. [10], heat pumps, e.g. Zhu et al. [11], and in other industry domains, e.g. Reddick et al. [12], there is an additional growing interest in studying carbon dioxide flashing flow in the converging-diverging nozzles and experimental data in this field are available. Studies on implementation of the ejectors with converging-diverging nozzles for refrigeration, air-conditioning and heat pumps demonstrated significant improvement of the energy efficiency of the discussed systems, Boccardi et al. [13] Liu et al. [14] Lucas et al. [15]. Since carbon dioxide critical temperature is relatively low, those applications concern cases where the supercritical fluid feeds the motive nozzle. Available experimental data with carbon dioxide provide an opportunity to study the prediction of two-phase critical flow through the converging-diverging nozzle since most of the previous analyses were carried out for water substance only.

The potential energy of pressure at the motive nozzle inlet is partly converted into kinetic energy during the flow in the discussed nozzle. The lower the pressure is at the motive nozzle outlet, the higher the motive stream velocity is, providing a better potential of momentum transfer with the secondary stream farther downstream. For given operation conditions (inlet and outlet pressures) the maximum achievable

velocity for a simple converging nozzle is the propagation velocity or the speed of sound as it was reported by Bilicki and Kestin [16]. For a converging-diverging nozzle, the velocity at the nozzle outlet could be larger and it depends on the geometry of the nozzle divergent part. Therefore, an accurate prediction of the local sound speed values is a crucial issue for an appropriate nozzle design. This problem was widely investigated, among others by: Bilicki and Kestin [16], Attou and Seynhaeve [17], Angielczyk et al. [18], Lorenzo et al. [19] and it was proved that most physically consistent predictions of the sound speed may be obtained from models that take into account the thermal non-equilibrium effects. One of this kind of models, namely Homogeneous Relaxation Model (HRM) was investigated in the previous paper of Angielczyk et al. [18]. However, it was shown by Bartosiewicz et al. [20] that Delayed Equilibrium Model (DEM), which is also a relaxation model and consequently it gives physically consistent prediction of the sound speed, is more accurate than HRM in terms of the critical mass flow rate prediction. DEM ability to accurately predict the critical mass flow rate was also confirmed by Lorenzo et al. [19] through confrontation with experimental data of a wide range (incorporating flows through long tubes, short tubes, and slits). The main conclusion of the above mentioned investigations is that among tested models (HEM, HRM and lumped parameter approach of Moody and Hanry-Fauske), DEM is the most accurate in terms of both the critical mass flow rate predictions and pressure distribution predictions.

Therefore, the main aim of the present investigation was to check if the Delayed Equilibrium Model with a closure law, originally developed for water, may be considered as suitable for modelling of CO_2 transonic two-phase flows. Homogeneous Equilibrium Model calculations have been used as a reference case and to verify whether the Lockhart-Martinelli and the Friedel approaches are suitable for calculations of a friction pressure drop in CO_2 transonic two-phase flows.

2. Homogeneous Equilibrium Model (HEM)

Attou and Seynhaeve [17] investigated the steady-state critical two-phase flashing flow with possible multiple choking phenomenon. One of the results of this investigation was a conclusion that HEM is not appropriate to accurately predict the sound speed for low quality flows but still this model is the simplest two-phase flow approach eligible for the small amplitude disturbances propagation analysis as it was presented by Bilicki and Kestin [16]. This analysis allows to determine an expression for the sound speed that is an intrinsic feature of the model. Among the two-phase flow models, HEM is distinguished by the smallest number of closure equations. Namely, it requires only an equation for the transferred heat flux q and an equation for the wall shear stress τ. It is also related to an instantaneous mass transfer between fluid fractions. For those reasons, HEM is commonly treated as a reference case. It is also used as a reference case in this investigation.

HEM imposes the thermal equilibrium between vapour phase and liquid phase. Consequently, the temperatures and pressures of both phases are equal. It also assumes that phases are uniformly distributed (perfectly mixed), that results in equal velocities and mechanical equilibrium. The model consists of three conservation equations of mass, momentum, and energy, respectively:

$$w\frac{d\rho}{dz} + \rho\frac{dw}{dz} = -\rho w\frac{1}{A}\frac{dA}{dz}, \tag{1}$$

$$\frac{dp}{dz} + \rho w\frac{dw}{dz} = -\frac{\tau C}{A}, \tag{2}$$

$$\rho w\frac{dh}{dz} - w\frac{dp}{dz} = w\frac{\tau C}{A} + \frac{qC}{A}. \tag{3}$$

Those equations have to be supplemented with the following state equations describing the specific volume (or density) and the specific enthalpy of the two-phase mixture:

$$v = \rho^{-1} = (1-x)v_{sl} + xv_{sg}, \tag{4}$$

$$h = (1-x)h_{sl} + xh_{sg}. \tag{5}$$

Since the quantities with subscript *sl* and *sg* represent saturated liquid and saturated vapour properties, respectively, which are functions only of the pressure p, then the system contains three independent variables. Those three variables could be freely selected. In the implementation of HEM used in this investigation, the independent variables are: the pressure p, the quality (the saturated vapour mass fraction) x, and the velocity w. Since the flow is assumed to be adiabatic then the heat flux q is equal to 0.

3. Delayed Equilibrium Model (DEM)

DEM assumes existence of three fractions: the metastable liquid phase (subscript *ml*), the saturated liquid phase (subscript *sl*), and the saturated vapour phase (subscript *sg*). The saturated fractions are in thermal equilibrium so that they have equal pressures and temperatures. The metastable fraction is assumed to have the same pressure as the saturated phases but higher temperature, as it is usually assumed to be frozen or proceed an isentropic expansion. Therefore, DEM takes into account the thermal non-equilibrium effects but it does not include the mechanical non-equilibrium effects. DEM consists of the conservation Eqs. (1–3) substituted with the following state equations:

$$v = (1-y)v_{ml} + (y-x)v_{sl} + xv_{sg}, \tag{6}$$

$$h = (1-y)h_{ml} + (y-x)h_{sl} + xh_{sg}. \tag{7}$$

On the basis on Eqs. (6) and (7) there can be inferred that the vaporisation index y is simply the mass fraction of the saturated phases, thus it depends on three mass flow rates:

$$y = \frac{m_{sl} + m_{sg}}{m_{ml} + m_{sl} + m_{sg}} = \frac{m_{sl} + m_{sg}}{m}. \tag{8}$$

In order to complete the model a mass balance equation for one of the three phases has to be added to the system of Eqs.: (1–3), (6), (7). Originally, DEM was developed in purpose to simulate choked two-phase water flows. Thus, this closure equation describes the evolution of water saturated fractions during the flashing process. Recently, the closure equation has been presented by Seynhaeve et al. [21] and Lorenzo et al. [19] in the following form:

$$\frac{dy}{dz} = (C_1\frac{C}{A} + C_2)(1-y)\left[\frac{p_s(T_{ml}) - p}{p_c - p_s(T_{ml})}\right]^{C_3},$$
$$C_1 = 0.008390,\ C_2 = 0.633691,\ C_3 = 0.228127 \tag{9}$$

The implementation of DEM used in this investigation treats the flow as adiabatic ($q = 0$). The metastable fraction is subjected to an isentropic expansion. The independent variables are: p, x, y, w.

4. Solution procedure

In a case where the nozzle inlet is fed with fluid in its supercritical or subcooled state a single-phase flow model has to be applied prior to a two-phase flow approach. The single-phase flow model consists of system of equations, Eqs. (1–3), supplemented with state equations describing the supercritical or subcooled properties of the fluid (equation developed by Span and Wagner [22], has been used here). This model operates until the saturation conditions are reached. Subsequently, a two-phase flow model (e.g. HEM or DEM) could be applied.

As long as the expansion leads from the supercritical state (through subcooled states) into the saturation state, the flow is subsonic and the single-phase flow model solutions could be determined by conventional forward-marching integrations. However, determination of the transonic solutions (either of a two-phase flow model or gas flow model) requires a profound topological analysis. This analysis uses the

theory of dynamical systems and was conducted by Bilicki et al. [16, 23]. This section presents only crucial elements of the analysis which are necessary to clearly describe the applied solution procedure. The proposed methods require some information that can be obtained by applying the Possible-Impossible Flow algorithm. Therefore, this approach has been also briefly described in this section.

4.1. Topological structure of the phase space

Practically all known one-dimensional models of a steady-state flow (including HEM and DEM) can be presented in a form of the following nonlinear ordinary first order differential equation system (Einstein summation convention has been applied):

$$A_{ij}(\sigma)\frac{d\sigma_i}{dz} = b_i j(z, \sigma), \ (i, j = 1, 2, \ ..., n). \tag{10}$$

The size and elements of matrix A and vector b depend on the model type. The vector σ consists of n quantities describing thermodynamic state of the fluid, and if necessary, velocity of the fluid (in this case it is called a velocity-state vector). The elements of matrix A depend only on vector σ components, and vector b elements additionally depend on the spatial coordinate z. The set of governing Eq. (10) supplied with vector $\sigma_B = [\sigma_{1,B}, \sigma_{2,B}, \ldots, \sigma_{n,B}]$ (related to the flow inlet conditions, the inlet is located at z_B) creates an initial-value problem. A solution to the problem is a trajectory $\sigma(z)$ in $n+1$ dimensional phase space Ω. Vector $[dz, d\sigma_1, d\sigma_2, \ldots, d\sigma_n]$ is tangent to $\sigma(z)$ at each point. Therefore, vector V defined as:

$$\left[\frac{dz}{dt}, \frac{d\sigma_1}{dt}, \frac{d\sigma_2}{dt}, \cdots, \frac{d\sigma_n}{dt}\right] = [D, N_1, N_2, \cdots, N_n], \tag{11}$$

is also tangent to $\sigma(z)$. Here D denotes a determinant of the A matrix, and N_i are determinants of matrices that are created by replacing the i-th column of A with b. It is worth to notice that Eq. (11) is an autonomous form of the system (10) and that in this autonomous form the independent variable is not z but the dummy parameter t. Fig. 2 presents a projection of trajectories corresponding to flows through a converging-diverging nozzle on pressure p - spatial coordinate z plane ($\sigma_1 = p$). The inlet conditions related to those flows differ only in the velocities. Consequently, all trajectories related to the curves in Fig. 2 start form the same values of the inlet pressure p_B, density ρ_B, and specific enthalpy h_B.

The trajectory that corresponds to a fully subsonic flow can be determined through a numerical forward-marching integration of Eqs. (10) or (11) from the inlet conditions towards the nozzle outlet (e.g. by using of Euler or Runge-Kutta methods with adaptive integration step). Fig. 2 presents projections of three subsonic trajectories (the curves passing through points M, O, R). Those kinds of trajectories are called possible flow (PF) solutions. The PF trajectories consist of only regular points, which means that on those trajectories $D \neq 0$. The trajectories related to curves passing through points F, G, H are called impossible flow (IF) solutions. At those points, the fluid velocity reaches the local sound speed. Consequently, at those points $D = 0$ and they are called turning points. Providing that the autonomous form of Eq. (11) is used, these trajectories are not problematic for conventional numerical integration methods either.

The trajectory related to the curve passing through points B, S, E_1 is the sought transonic solution. Point S at which $D = 0$ and all $N_i = 0$ is a singular point. The direction of V at this point is undefined because its magnitude is equal to 0. Let us denote this point by $S = (z_S, \sigma_{1,S}, \sigma_{2,S}, \ldots, \sigma_{n,S})$. According to (11), $dz = D\,dt$ and $d\sigma_i = N_i\,dt$. Therefore, at singular points the values of Δz and $\Delta\sigma_i$ calculated by the numerical integration methods are equal to zero regardless of the integration step size Δt. It means that the numerical integration algorithms cannot neither "start from" nor "pass through" this kind of points. Therefore, another approach is required that is different than forward-marching integration.

The conventional solution to this problem is based on the fact that when S is a singular saddle point then the eigenvectors of the Jacobian of V are tangent to the trajectories that pass through S (the Jacobian has to be calculated at the point S). The point S is a singular saddle point when eigenvalues associated with the eigenvectors are real numbers of opposite signs (otherwise, S is a singular spiral point or a singular nodal point but those cases are beyond the scope of this investigation). Let us denote the eigenvector tangent to the transonic trajectory by V_1 (Fig. 2). Making a step along V_1 determines a point that is eligible for starting numerical integration. The up-stream integration when it reaches z_B, determines the inlet conditions corresponding to the considered singular saddle point. Similarly, down-stream integration determines the outlet conditions. Therefore, the described procedure is actually a solution to an initial-value problem of equations system (11) with initial values: $z = z_S$ and $\sigma = \sigma_S$. In this conventional approach, the singular saddle point is chosen arbitrarily. Thus, in general case, the corresponding inlet conditions significantly differ from the given values.

In order to fit into the given inlet conditions, a shooting method (that starts from singular saddle point) can be applied, e.g. method described in handbook of Press et al. [24]. If the shooting method utilises multidimensional, globally convergent Newton-Raphson algorithm then the approach is called Newton Critical Point method (NCP). A detailed description of NCP was presented by De Sterck [25]. Each NCP iteration requires n integrations to determine how to change n-1 singular saddle point parameters, handbook of Press et al. [24]. The enormous overall integration number makes this method relatively slow (especially if compared to Possible-Impossible Flow algorithm). The described issues and the laboriousness of solving the V Jacobian eigenvalue problem was a motivation for developing a faster approach.

4.2. Possible-Impossible flow algorithm (PIF)

In fact, the PIF algorithm is not able to determine the sought transonic trajectory, but with each PIF iteration, the region of phase space that contains the sub-sonic part of the sought trajectory is narrowed down. Thus, in theory, this trajectory part could be localised in an arbitrarily small region of the phase space. In practice, the numerical errors preclude to restrict the region arbitrarily. The idea of PIF is based on the fact that the sought transonic trajectory lies between PF and IF trajectories (Fig. 2). As it was mentioned in the previous section, those trajectories can be easily obtained by numerical forward-marching integration of the equations system (11). The PIF algorithm has been widely used, among others by Boure et al. [26], Feburie et al. [27], Bolle et al. [28], Downar-Zapolski et al. [29], Attou and Seynhaeve [17], Lorenzo et al. [19] in the form that can be described in the following steps:

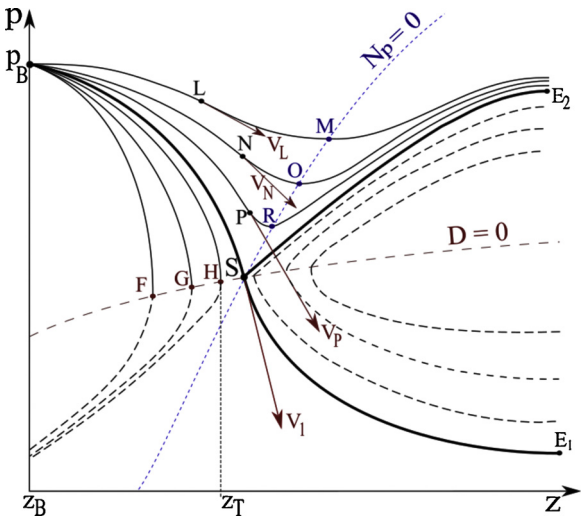

Fig. 2. Projection of solutions to the initial-value problems on p - z plane.

1 Calculate an intermediate mass flow rate $m = (m_{PF} + m_{IF})/2$ and related inlet velocity w.
2 Integrate equations system (11) from the inlet conditions (p_B, ρ_B, w) and at each step check if D has changed sign.
3 If D has changed its sign before the end of the channel then assign the value of m to m_{IF}.
4 If D has not changed its sign before the end of the channel then assign the value of m to m_{PF}.
5 If m_{IF}-m_{PF} is low enough then stop, otherwise go to point 1.

This form of PIF is general in terms of the channel geometries that it can be applied to. However, if the channel cross-section area has only one or has no minimum (convergent-divergent nozzles, convergent nozzles, pipes with abrupt enlargement, constant area ducts) much faster implementation can be used. This implementation bases on the following consideration: Let us notice that on PF trajectories D does not change sign and that on IF trajectories Ns do not change signs (Fig. 2). Thus, instead of integrating, in each PIF iteration, up to the channel outlet, it is better to check both D and one of Ns sings at each integration step. If only D has changed its sign, then it is IF. If only chosen N_i has changed its sign, then it is PF. If both have changed their signs, then it is necessary to repeat the current integration iteration with a smaller integration step. With the exception of a singular saddle point, Ns never change the signs at the same point on the trajectory. Consequently, the choice of N_i matters, but not significantly. Own authors experience is that N_p changes sign first, thus utilisation of this determinant is usually the best choice.

4.3. Proposed generalised method of singular saddle point determination

The proposed method utilises the fact that the saddle singular point is an intersection point of the following curves: $D(\sigma) = 0$, $N_i(z,\sigma) = 0$ (Fig. 2 shows curve $D = 0$ and $N_p = 0$). Thus, determination of the saddle singular point approximation requires the following steps (the PIF procedure has to be conducted previously):

1 Approximate the curve $D(\sigma) = 0$ by the straight line passing through point G and H.
2 Determine a point $S_i(z_i,\sigma_i)$ that lies on the line. At this point$z_i = z_H + \Delta z$. Assume that $m_i = m_H + \Delta z(m_H\text{-}m_G)/(z_H\text{-}z_G)$. = zH + z. Assume that mi = mH + .
3 Use the gradient descent method (take S_i as a starting point) to determine $S_{i0}(z_i,\sigma_{i0})$ where $D = 0$.
4 If all Ns at the point S_{i0} have different signs than in the point H, then repeat the previous steps with smaller Δz until the required accuracy is reached. Otherwise, repeat the previous steps but replace H with S_{i0}.

The gradient descent method (also called steepest descent method) is a first-order iterative optimisation algorithm for finding the minimum of a function, see Press et al. [24]. However, here the algorithm was used to find σ_{i0} at which $D = 0$. This is based on the fact that between starting point where $D > 0$ and point where D has a negative minimum value there is a point at which $D = 0$.

The proposed method is generalised in the sense that it may be applied for any model described by Eq. (10) regardless of the equations number. The singular point found by means of the above algorithm corresponds to certain inlet conditions. Those conditions may be thought as the better approximation of the original inlet conditions (Fig.2, point B) since the points G and H are located closer to the point S. In the other words, the higher number of PIF iterations, the better accuracy of the solution.

4.4. The transonic trajectory

Fig. 2 shows the points L, N, P that are inflection points of the subsonic trajectories. Each of the vectors V_L, V_N, V_P is tangent to a trajectory at a corresponding inflection point. The points M, O, R represent local pressure minima. It is worth to notice that the closer to the point S the subsonic trajectory lies, the closer the inflection point of this trajectory is to the pressure minimum point of this trajectory. Finally, at the transonic trajectory those points merge together into point S. Consequently, the direction of V_1 can be approximated by the direction of V_P. The higher number of PIF iterations, the smaller distance between points R and S and the better accuracy of the V_1 direction approximation. The direction of V_P can be directly used to carry out the integration from the found saddle singular point (as it was described in the Subsection 4.1) giving an approximation of the subsonic and supersonic parts of the sought transonic trajectory. Nevertheless, the higher accuracy can be reached by using V_P as a first guess for well-known iterative methods of eigenvector determination, e.g. inverse power method, see Press et al. [24].

5. The experimental data

The unique experimental data concerning two-phase transonic carbon dioxide flow through a nozzle were published by Nakagawa et al. [30]. The experiment was made through a blown-down test of CO_2. The investigated nozzle was fed from CO_2 tank and after passing through the nozzle, CO_2 was exhausted to the atmosphere. Converging-diverging stainless steel nozzles were used in the experiment. All used nozzles had a rectangular cross-section area. The throat cross-section area was 0.24 mm × 3 mm. During all tests the width of the nozzle (3 mm) and the lengths of converging and diverging sections (27.35 mm, and 56.15 mm, respectively) were unchanged. Divergence angle α was changed, and for each nozzle geometry the pressure distribution in the diverging nozzle section was measured by means of four strain gauges. Also, the fluid temperature distribution was measured by means of nine taps. The geometry of the experimental nozzles is presented in Fig. 3 and Table 1.

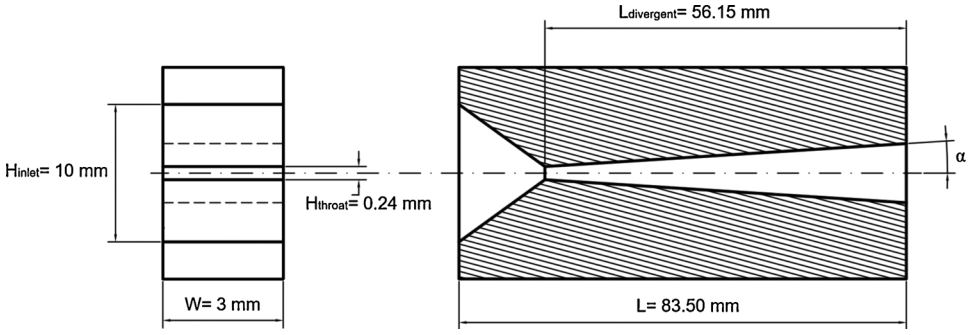

Fig. 3. Geometry of the experimental nozzle.

Table 1
Variable parameters of the experimental nozzles.

Nozzle number	Divergent part angle α		Outlet cross-section area [mm^2]
	[rad]	[°]	
1	0.0013	0.077	1.17
2	0.0026	0.153	1.62
3	0.0053	0.306	2.52
4	0.0107	0.612	4.32

6. Results

The initial goal of this investigation was to check whether the correlation for the evolution of the vaporisation index dy/dz, originally developed with DEM for water choked flows, is suitable for CO_2 transonic flows. However, also some DEM adjustment attempts were carried out but the results were unsatisfactory (Table 2). An additional analysis that reveals the reasons for the failure is presented in Subsection 6.2.

6.1. DEM results compared with HEM predictions

The DEM correlation constants presented in Eq. (9) were adjusted on the base of the Super Moby Dick experiment simulations described for instance by Lorenzo et al. [19]. The Super Moby Dick experiment concerns water choked flows through short and long nozzles. It contains database of pressure and void fraction profiles along with related critical mass flow rates. In the simulations, the model has been supplemented with Darcy friction factor calculated on the base of the Lockhart–Martinelli (LM) parameter and the flow was treated as adiabatic [19].

As a first step of the investigation, calculations of all 10 runs of CO_2 flow cases presented by Nakagawa et al. [30] were carried out with described DEM original setup. In addition, calculations with use of HEM were carried out in order to obtain the reference data that are related to an instantaneous mass transfer between the considered fluid fractions. After the preliminary calculations, two experimental cases (related to the supercritical inlet conditions and small angles of the nozzle divergent part) were excluded from the investigation as they turned out to be cases of a single-phase flow.

All calculated two-phase flow cases, related to the described original DEM setup but conducted for CO_2, revealed the same tendency. This tendency (for sake of clarity) is here presented on the basis of only three flow cases. Those representative cases cover the whole range of the investigated inlet conditions (9.1 MPa, 7.1 MPa, 6.1 MPa) and revealed significantly different localisation of the critical section. Pressure profiles for those cases are plotted in Figs. 4, 6, and 8 with red dashed lines and denoted by DEM. The related quality (vapour mass fraction) profiles are presented in Figs. 5, 7, and 9, respectively.

In the first of the representative cases, shown in Fig. 4, the inlet conditions describe a point in a supercritical region ($p_{in} > p_c$, $T_{in} > T_c$). In this case the nozzle outlet area (and consequently the angle of the nozzle divergent part α) is the highest one. Thus, a strong decompression was expected to occur in the nozzle divergent part (as described by the experimental data or any of the HEM implementations). However, DEM generates a pressure profile located above the experimental pressure distribution despite the corresponding mass flow rate m_{DEM} is much higher than those calculated by means of any of HEM implementations (Fig. 4). The critical section (where the fluid velocity reaches the local sound speed, consequently $D = 0$), in this case, is located quite away from the throat ($z_S \approx 0.0353$ m) and contains a singular saddle point (thus, at this location also $N_i = 0$). The shift of the critical section downstream from the throat is caused by a presence of thermal none-equilibrium and friction terms in the system of Eqs.: (1–3), (6–9). This effect was described, among others, by Bilicki et al. [16, 23]. In general, all dissipative phenomena that are included in the flow model (friction losses, none-instantaneous interphase mass transfer and also an external heat transfer, which here is neglected) result in shifting the critical section downstream beyond the throat. Also, a decrease in the nozzle divergent part angle α would result in shifting the critical section downstream. The influence of the non-instantaneous mass transfer on the phenomenon can be explained through an analysis of Eqs. (1) and (2). The cross-section area of the nozzle begins to increase ($dA/dz > 0$) after the throat. In case of a flow that at this point is subsonic, this kind of geometry change tends to deaccelerate the fluid and to increase the pressure ($dw/dz < 0$, $dp/dz > 0$). However, if the pending vaporisation process provides a sufficient mixture density drop gradient ($d\rho/dz << 0$, for sufficient compressibility of the fluid), the acceleration continues and the mixture velocity reaches the local sound speed value somewhere after the throat. Naturally, the acceleration directly after the throat (and also the location of the critical section) depends on both dA/dz and $d\rho/dz$. If the mixture density drop gradient is the same or lower than it is before the throat ($d\rho/dz$ is less negative), then after the throat pressure drop gradient is also lower (dp/dz is less negative) than before the throat. The red dashed line between the throat and the singular saddle point (Fig. 4) illustrates the described effect. In this case, the pressure drop gradient is so low that the pressure at some distance seems to be constant. It happens due to the application of the original form of the closure law, Eq. (9), that strongly restricts the interphase mass transfer rate.

The described pressure drop gradient decrease occurs in any case (also in HEM distributions) but it is more visible when the critical section is noticeably shifted beyond the throat. Since HEM does not incorporate any of non-equilibrium effects then the shift is caused merely by the friction losses and usually it is negligible. However, the friction losses are substantial (and occur in the nozzle with sufficiently low divergent part angle) in HEM-LM flows presented in Figs. 10–14 and HEM-Friedel flow presented in Fig. 10. In those cases, the critical section is shifted until the nozzle outlet.

In case of the reference HEM profiles (Fig. 4, HEM-LM) the Darcy friction factor is also calculated by means of LM parameter. The singular saddle point is located beyond the throat but so close to the throat that it cannot be distinguished in the figure of applied scale. The curve representing a supersonic part of the trajectory starts from the singular saddle point and it is fully convex until the nozzle outlet. The quality distributions (Fig. 5) demonstrate that the original form of Eq. (9) restricts the interphase mass transfer rate so strongly that, despite the highest mass flow rate, DEM produces the least steep quality profile.

Table 2
Discrepancies between experimental and calculated pressure values for the case presented in Fig. 4.

z [mm]	DEM		DEM-CO_2-LM		HEM-LM		HEM-Friedel		HEM-izentropic	
	δ [MPa]	δ_r [%]	δ [MPa]	δ_r [%]	δ [MPa]	δ_r [%]	δ [MPa]	δ_r [%]	δ [MPa]	δ_r [%]
37	−1.6626	−41.39	−0.5670	−19.41	−0.5672	−19.42	0.2415	11.43	0.4375	22.83
47	−1.4517	−51.05	−0.4669	−25.11	−0.4670	−25.12	0.0669	5.05	0.2529	22.21
57	−1.3323	−61.71	−0.5172	−38.48	−0.5173	−38.49	−0.1327	−13.83	0.0363	4.59
67	−1.2820	−74.47	−0.6076	−58.03	−0.6076	−58.03	−0.3118	−41.50	−0.1575	−26.38

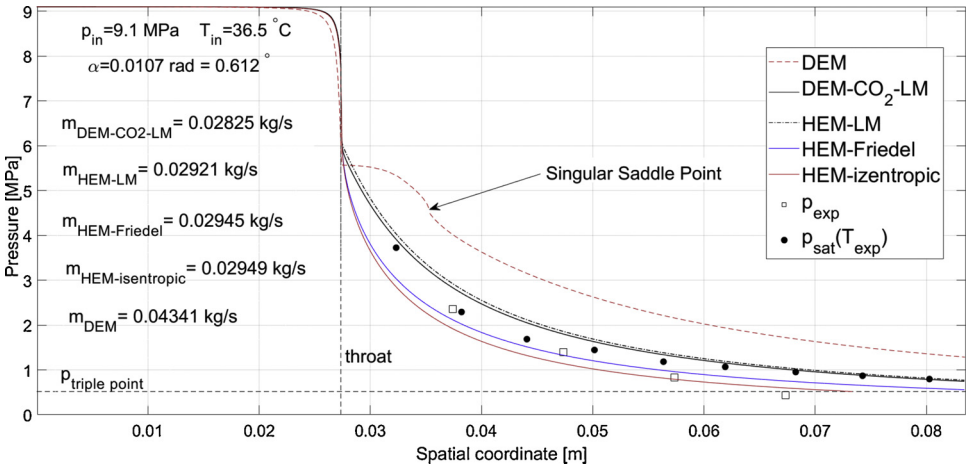

Fig. 4. Calculated pressure profiles of Nakagawa et al. blow-down CO_2 experiment for supercritical inlet conditions (9.1 MPa, 36.5 °C).

The same tendency appeared in all investigated experimental flow cases but for clarity reasons only the remaining representative cases were depicted, see Figs. 7 and 9.

The second representative case is presented in Fig. 6. Again, the generated DEM pressure profile is located high above the experimental pressure distribution, despite the corresponding mass flow rate m_{DEM} is much higher than those calculated by means of any of HEM implementations. However, the singular saddle point is located almost in the middle of the nozzle divergent part. Consequently, the related trajectory is fully convex from this point until the nozzle outlet.

The last representative case is presented in Fig. 8. The generated DEM pressure distribution is still above the experimental data. The corresponding mass flow rate is still the greatest but the critical section in this case is located at the nozzle outlet and contains a turning point. Consequently, the trajectory in the divergent part of the nozzle cannot be fully convex.

The provided calculations results reveal that the original DEM setup is not suitable to correctly predict CO_2 pressure profiles of Nakagawa et al. [30] experiment. The calculated profiles are passing above the experimental points. Thus, it seems that the dy/dz (rate of the saturated phases production) calculated by the original form of Eq. (9) is too low for the case of CO_2 flows. In the previous work, Angielczyk et al. [18], the same conclusion was drawn on the base of HRM preliminary calculations. Consequently, in order to increase the saturated phase production, the non-equilibrium effects were restricted by decreasing the relaxation time values. In the case of DEM, an increase of dy/dz requires higher values of C_1, C_2 in Eq. (9). The results (presented in Figs. 4, 6 and 8 by black solid lines) confirmed the conclusion concerning dy/dz, since the curves calculated for the new set of the constants (which is: $C_1 = 5.17$, $C_2 = 0.87$ and $C_3 = 0.25$) are passing closer to the experimental points. It is worth to notice that the new constant values of C_1 and C_2 are significantly higher than those obtained for water ($C_1 = 0.00839$, $C_2 = 0.633691$, $C_3 = 0.228127$). Moreover, the further calculations with application of even higher constants produced the curves that pass slightly closer to the experimental points. However, this improvement has a limitation. Namely, when dy/dz is sufficiently high then DEM calculations result with pressure profiles (DEM − CO2-LM in Figs. 4, 6, 8) almost identical with those produced by corresponding HEM implementation (HEM-LM). The discrepancies between experimental and calculated pressure profiles are presented in Table 2 and they correspond to the flow depicted in Fig. 4. However, the most important conclusions arising from the analysis of Table 2 are identical for all flow cases. Namely:

- the strongest deviation from experimental data reveals DEM,
- DEM-CO2-LM and HEM-LM are giving practically the same discrepancies.

This situation is caused by a fact that when DEM operates with significantly high dy/dz values, only few integration steps are required to fully convert the metastable fraction into saturated fractions and as a result DEM starts to produce results similar to HEM. Nevertheless, these few steps introduce a small discrepancy between models predictions which is caused by a fact that the metastable fraction (that undergoes

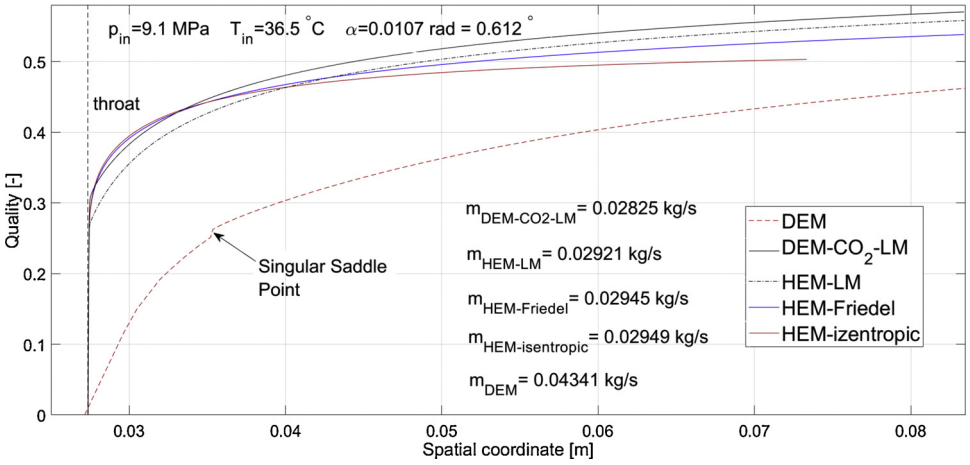

Fig. 5. Calculated quality profiles of Nakagawa et al. blow-down CO_2 experiment for supercritical inlet conditions (9.1 MPa, 36.5 °C).

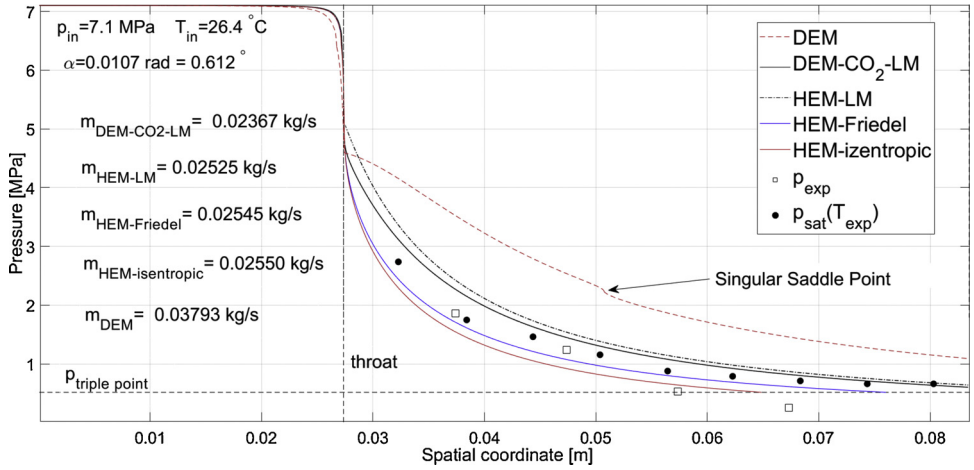

Fig. 6. Calculated pressure profiles of Nakagawa et al. blow-down CO_2 experiment for barely subcritical inlet conditions (7.1 MPa, 26.4 °C).

an isentropic expansion) has a higher temperature than the saturated fractions. Consequently, the density of this fraction is lower than the density of the saturated liquid fraction. Thus, the overall density defined by Eq. (6) is lower than the corresponding homogeneous equilibrium mixture density. Therefore DEM-CO_2-LM predicts slightly lower mass flow rates than HEM-LM. Unfortunately, the accuracy of those predictions cannot be verified since the experimental data of Nakagawa et al. [30] do not contain values of mass flow rates related to the presented experimental pressure distributions. The further increase of dy/dz leads to a case in which the metastable fraction disappears in just one integration step. In this case, the deviation of DEM-CO_2-LM from HEM-LM is the lowest. For even higher dy/dz values the integration algorithm significantly decreases the integration step. Finally, the step is so small and dy/dz is so high that the related numerical errors are huge and the algorithm produces physically irrelevant trajectories.

The presented limitation of DEM adjustment seems to prove that the non-equilibrium effects do not play a role in the investigated CO_2 flows and consequently, those flows can be described by HEM. Unfortunately, this is not a case, since HEM pressure profiles are not even close to the experimental distributions for flows through nozzles of low divergent angles $\alpha = 0.077^\circ$ and $\alpha = 0.153^\circ$.

Actually, the impossibility of the adjustment of the constants of Eq. (9) in such a way that the DEM pressure profiles would pass significantly under the corresponding HEM-LM profiles (consequently, closer to the experimental distributions) with physically realistic values of dy/dz, proves that there are the other factors than dy/dz that have an essential influence on the process and they need to be further recognised and investigated.

6.2. HEM results and the impact of the friction factor approach

Some unexpected conclusions may be drawn from analysis of HEM curves (Figs. 4, 6, 8 black doted-dashed lines). Namely, in all of the cases the HEM curves pass above the saturated pressure points (black dots) that are calculated for measured temperatures. However, this situation is not physically accurate. Let us consider an approximation of the flowing fluid as a mixture of two saturated fractions and not one but many metastable fractions. In this case, the "hottest" metastable fraction has temperature T_{ml}. The remaining metastable fractions have lower temperatures and the saturated fractions have the lowest temperature T_s ($T_{ml} > T_{ml,1} > \ldots > T_{ml,n} > T_s$). Therefore, the measured temperature can be at most equal to T_{ml} and at least equal to T_s. Thus, the physically realistic HEM profiles always pass under the black dots. Only in such a case, an introduction of the non-equilibrium effects could produce a temperature profile that realistically corresponds to the measured temperatures.

The only changeable relations in HEM are those for the wall shear stress τ and the heat flux q. The second one is assumed to be zero what is justified for short nozzles as the investigated [17]. Thus, in order to understand the problem, it is reasonable to investigate an influence of the Darcy friction factor calculation approaches (indirectly, also impact of τ since Darcy friction factor is related to τ). The reference model is HEM with $\tau = 0$ (denoted by DEM-isentropic), which due to admitted assumptions ($\tau = 0$, $q = 0$) describes an equilibrium–isentropic process

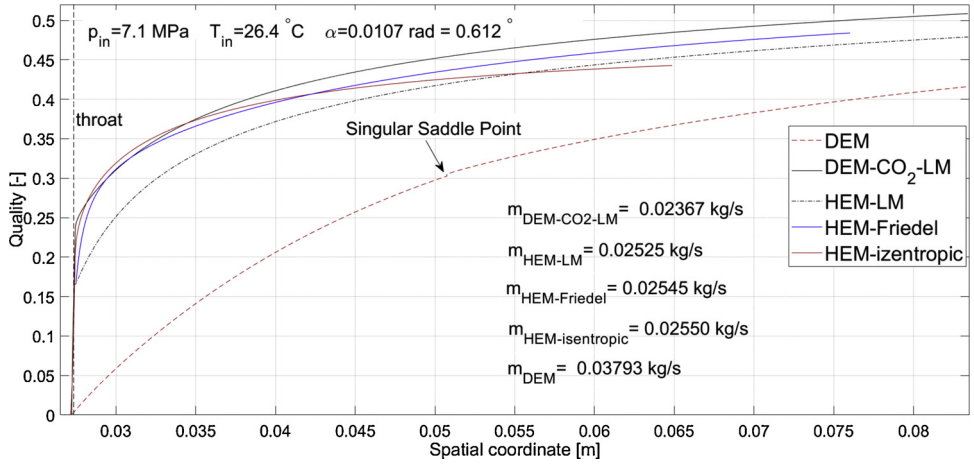

Fig. 7. Calculated quality profiles of Nakagawa et al. blow-down CO_2 experiment for barely subcritical inlet conditions (7.1 MPa, 26.4 °C).

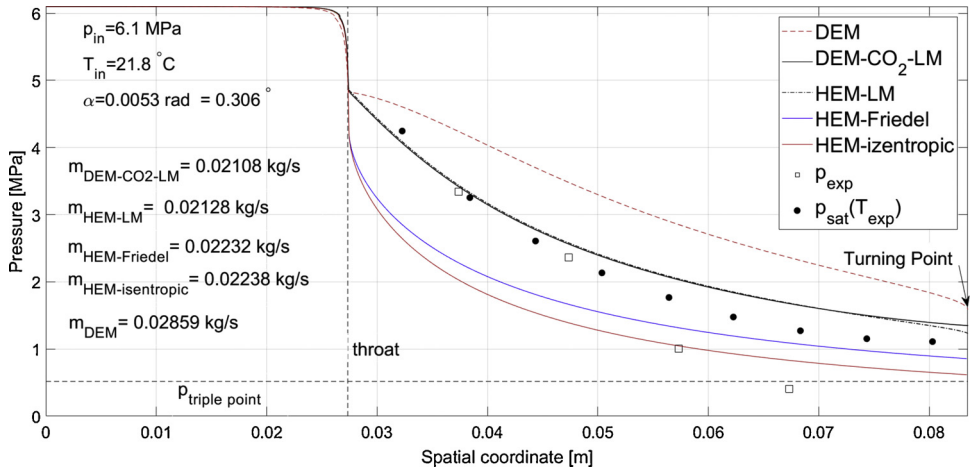

Fig. 8. Calculated pressure profiles of Nakagawa et al. blow-down CO_2 experiment for subcritical inlet conditions (6.1 MPa, 21.8 °C).

of the possibly highest rate of the fluid velocity increase and the possibly lowest vapour phase production. The other investigated HEM implementations should use well-known approaches of the friction factor determination.

Aakenes et al. [31] have carried out a comparison of different approaches of friction factor calculations with CO_2 experimental data. The main conclusion of this investigation is that, among the investigated approaches (homogeneous friction-model, Friedel and Cheng approaches), the Friedel approach is the most suitable for the case of CO_2. Therefore, this approach is also investigated here together with broadly used LM approach. The selection of LM approach is natural since it was applied in DEM original setup but it is also interesting to test it since it was not investigated by Aakenes et al. [31]. The results of the investigation are presented in Figs. 4–14. In all cases, the pressure distributions calculated with LM approach (excluding single points of the experimental distributions presented in Figs. 8, 12, and 14) pass above the saturated pressure points (black dots) that are calculated for measured temperature values. Consequently, the LM method commonly used for water flows may be considered as improper for CO_2 flows. It is worth to note that the corresponding mass flow rate is the lowest one in all of the cases. In the cases presented in Figs. 4, 6, and 12 the singular saddle points are located slightly beyond the throat. As a result, the representations of the supersonic parts of the trajectories are fully convex. In the remaining cases, the critical sections are located at the nozzle outlet and they contain the turning points. The trajectory containing turning point cannot be fully convex in the divergent part of the nozzle as it was shown by Bilicki and Kestin [16].

It is worth to notice that all HEM implementations in Figs. 5 and 7 give similar quality distributions (the curves are smooth and pass through comparable quality values). However, in the case presented in Fig. 9 the curves related to HEM-LM and DEM-CO2-LM are not smooth like the remaining curves. The dx/dz gradient significantly changes magnitude just after the throat. This happens because both flows are subsonic until the nozzle outlet. Therefore, it is the result of the phenomenon that was already explained in the previous section. In Figs. 4–7 some HEM profiles terminate before reaching the nozzle outlet. It is due to reaching the triple point pressure. Thus, further calculations require the application of a three-phase model (solid-liquid-vapour system) which exceeds the scope of this paper.

The calculations related to $\tau = 0$ are plotted with red solid lines and denoted by HEM-isentropic. In every case, those curves represent the steepest pressure drop and the highest mass flow rate. They always pass under the experimental distribution of saturation pressures (the black dots) but not always under points of the experimental pressure distributions (Figs. 4, 6, 8, 12). In all of the HEM-isentropic cases, the critical sections are located slightly beyond the throat and consequently, curves related to the supersonic trajectories are fully convex. The blue lines were determined by means of the Friedel approach and they are denoted by HEM-Friedel. In most cases, they pass under the experimental saturation pressure distributions. The corresponding mass flow rates are always between those related to HEM-isentropic and HEM-LM. Only in the case presented in Fig. 10 the critical section is located at the nozzle outlet and contains a turning point. The remaining cases are characterised by the singular saddle points localised slightly

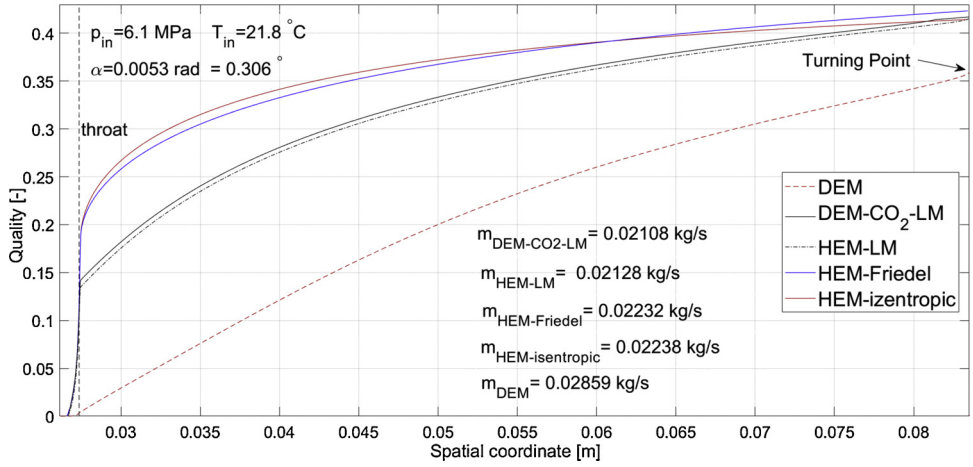

Fig. 9. Calculated quality profiles of Nakagawa et al. blow-down CO_2 experiment for subcritical inlet conditions (6.1 MPa, 21.8 °C).

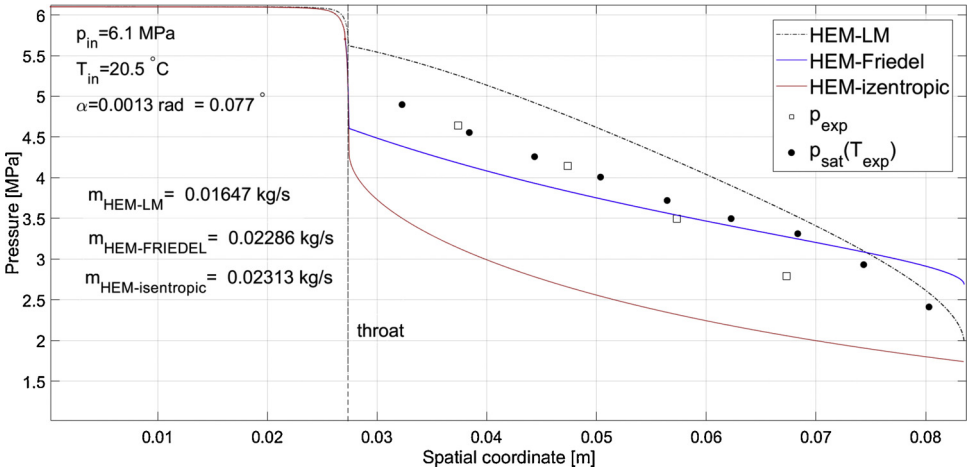

Fig. 10. Calculated pressure profiles of Nakagawa et al. blow-down CO_2 experiment for subcritical inlet conditions (6.1 MPa, 20.5 °C).

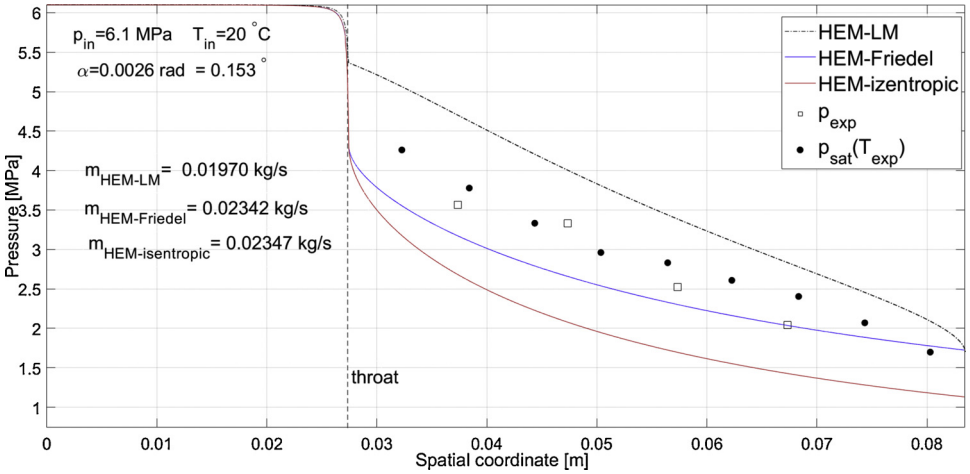

Fig. 11. Calculated pressure profiles of Nakagawa et al. blow-down CO_2 experiment for subcritical inlet conditions (6.1 MPa, 20 °C).

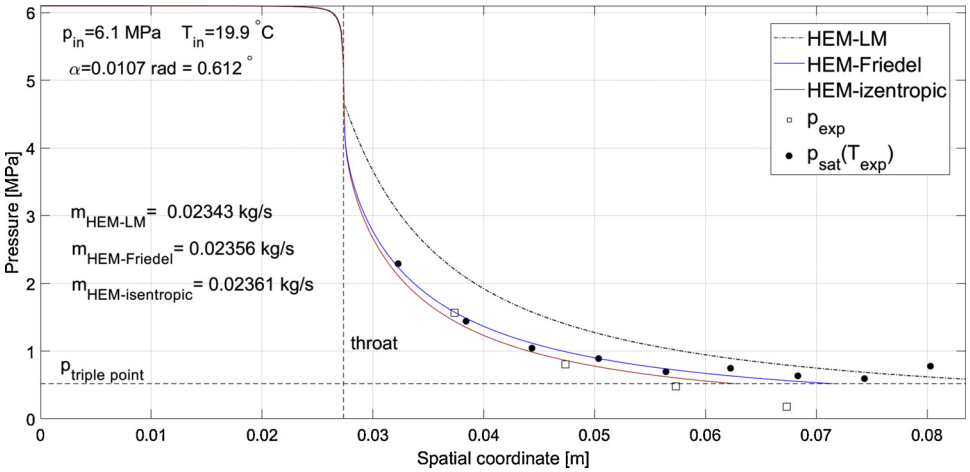

Fig. 12. Calculated pressure profiles of Nakagawa et al. blow-down CO_2 experiment for subcritical inlet conditions (6.1 MPa, 19.9 °C).

beyond the throat.

In summary, LM method turned out to be improper for CO_2 flows as it produces saturation pressure distributions that are passing above the saturated pressure points that are calculated for measured temperature values. In the case of Friedel approach, this situation happened only in three cases. Thus, this approach can be considered more appropriate for CO_2 flows. However, among the investigated HEM implementations, only HEM-isentropic produces saturation pressure distributions that are always passing under the saturated pressure points.

It was numerically confirmed that in most cases LM approach gives higher values of the friction factor then Friedel approach. Naturally, in the case of HEM-isentropic, the friction factor is equal to zero. Therefore, the comparison of the critical mass flow rates leads to a conclusion that the higher deviation from the isentropic process

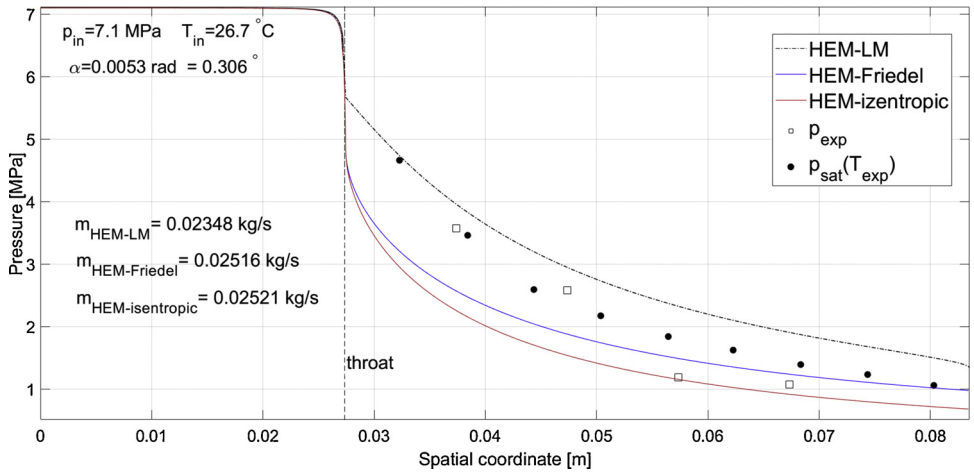

Fig. 13. Calculated pressure profiles of Nakagawa et al. blow-down CO_2 experiment for subcritical inlet conditions (7.1 MPa, 26.7 °C).

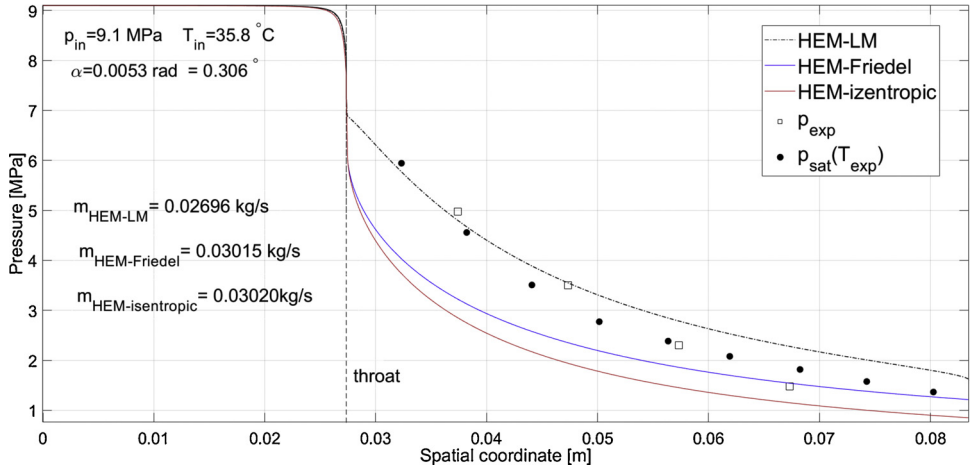

Fig. 14. Calculated pressure profiles of Nakagawa et al. blow-down CO_2 experiment for supercritical inlet conditions (9.1 MPa, 35.8 °C).

(towards the isenthalpic process) the lower critical mass flow rate. For a better understanding of this fact, it is worth to notice that during the isenthalpic process the vapour phase production is faster than in the isentropic case. Moreover, the local sound speed decreases drastically with the increase of the vapour mass fraction x, as it was reported by Downar-Zapolski et al. [29], Attou and Seynhaeve [17], Angielczyk et al. [18], Lorenzo et al. [19]. This leads to a conclusion that the higher deviation from the isentropic case, the lower mass flow rate is required to reach the local sound speed.

In the presented analysis it was assumed that the expansion process is adiabatic. However, even taking into account the possible heat transfer would result in the same final conclusions. Namely, Nakagawa et al. [30] reported that the ambient air temperature during tests was around 37 °C while the highest CO_2 inlet temperature was 36.5 °C. The fluid temperature decreases during the expansion process. Therefore, heat flows into the fluid and as a result the pressure drop required to evaporate the liquid decreases. It means that the ideally adiabatic flow would result in even lower pressures than the measured ones. Thus, in the considered case, the discrepancy between models predictions and the experimental data would be even higher. The same conclusion is obtained by consideration of the non-adiabatic flow model. In this case, q in Eq. (3) has to be higher than zero. As a result, process deviates towards isenthalpic expansion and the critical mass flow rate decreases resulting with less steep pressure profiles.

7. Conclusions

The presented investigations revealed that the original DEM setup developed for water is not suitable for CO_2 transonic flow calculations. Moreover, the attempt of adjusting the constants of Eq. (9) revealed that an increase of dy/dz causes an improvement of the pressure profiles predictions. However, this improvement is limited as a consequence of LM approach application.

The LM method turned out to be improper for CO_2 flows as it produces saturation pressure distributions that are passing above the saturated pressure points that are calculated for measured temperature values. In the case of Friedel approach, this situation happened only in three cases. Thus, this approach can be considered as more appropriate for CO_2 flows. However, among the investigated HEM implementations, only HEM-isentropic produces saturation pressure distributions that are always passing under the saturated pressure points. Therefore, DEM with $\tau = 0$ is the most reasonable implementation for further adjusting attempts of Eq. (9). This approach is planned to be used in the future works unless a more proper Darcy friction factor determination approach is found or developed. The presented HEM pressure profiles suggest that this kind of approach should produce values close to Friedel approach values (consequently, much lower than values given by LM approach) before and at the beginning of the nozzle divergent part and values close or even higher than those given by LM approach while approaching the nozzle outlet, regardless the location of the critical section.

The most recent works concerning the transonic CO_2 flows involve

2D or 3D Computational Fluid Dynamics approaches [6, 9, 10, 32, 33]. Therefore, it would be reasonable to compare their results with corresponding results of the presented 1D modelling approach. Thus, an importance assessment of 2D and 3D effects, based on such kind of comparison is planned as a next investigation step.

Another possible further step is a search for a CO_2 experimental database that (besides the pressure profiles) contains the values of critical mass flow rates since only this kind of data sets allow to carry out a reasonable model verification. However, the complete verification requires a database containing at least pressure profiles, void fraction profiles and critical mass flow rates which may be thought still as a challenge for experimentation technique.

References

[1] V.G. Pangarkar, Process intensification in multiphase reactors: from concept to reality, Chem. Eng. Process. Process. Intensif. 120 (2017) 1–8.

[2] S. Weber, S. Schaepe, S. Freyer, M.-H. Kopf, C. Dietzsch, Effect of ejector operation on the oxygen transfer in a pilot jet loop reactor, Chem. Eng. Process. Process. Intensif. 131 (2018) 43–50.

[3] F. Rahman, D.B. Umesh, D. Subbarao, M. Ramasamy, Enhancement of entrainment rates in liquid–gas ejectors, Chemical Engineering and Processing 49 (2010) 1128–1135.

[4] X. Gamisans, M. Sarrà, F.J. Lafuente, Fluid flow and pumping efficiency in an ejector-venturi scrubber, Chemical Engineering and Processing 43 (2004) 127–136.

[5] A.A. Abed, M.A. Alghoul, A.N. Al-Shamani, K. Sopian, Evaluating ejector efficiency working under intermediate pressure of flash tank–absorption cooling cycle: parametric study, Chemical Engineering and Processing 95 (2015) 222–234.

[6] M. Haida, J. Smolka, A. Hafner, M. Palacz, K. Banasiak, A.J. Nowak, Modified homogeneous relaxation model for the R744 trans-critical flow in a two-phase ejector, Int. J. Refrig. 85 (2018) 314–333.

[7] A. Attou, L. Bolle, J. Seynhaeve, Experimental study of the critical flashing flow through a relief line: evidence of the double-choked flow phenomenon, Int. J. Multiph. Flow 26 (6) (2000) 921–947.

[8] J.P. Janet, Y. Liao, D. Lucas, Heterogeneous nucleation in CFD simulation of flashing flows in converging–diverging nozzles, Int. J. Multiph. Flow 74 (2015) 106–117.

[9] M. Palacz, J. Smolka, W. Kus, A. Fic, Z. Bulinski, A.J. Nowak, K. Banasiak, A. Hafner, CFD-based shape optimisation of a co2 two-phase ejector mixing section, Appl. Therm. Eng. 95 (2016) 62–69.

[10] J. Smolka, M. Palacz, J. Bodys, K. Banasiak, A. Fic, Z. Bulinski, A.J. Nowak, A. Hafner, Performance comparison of fixed- and controllable geometry ejectors in a co2 refrigeration system, Int. J. Refrig. 65 (2016) 172–182.

[11] Y. Zhu, Y. Huang, C. Li, F. Zhang, P.-X. Jiang, Experimental investigation on the performance of transcritical CO2 ejector–expansion heat pump water heater system, Energy Convers. Manage. 167 (2018) 147–155.

[12] Ch. Reddick, M. Sorin, H. Sapoundjiev, Zine Aidoun, Effect of a mixture of carbon dioxide and steam on ejector performance: an experimental parametric investigation, Exp. Therm. Fluid Sci. 92 (2018) 353–365.

[13] G. Boccardi, F. Botticella, G. Lillo, R. Mastrullo, A.W. Mauro, R. Trinchieri, Experimental investigation on the performance of a transcritical CO2 heat pump with multi-ejector expansion system, Int. J. Refrig. 82 (2017) 389–400.

[14] F. Liu, E.A. Groll, J. Ren, Comprehensive experimental performance analyses of an ejector expansion transcritical CO2 system, Appl. Therm. Eng. 98 (2016) 1061–1069.

[15] C. Lucas, J. Koehler, A. Schroeder, C. Tischendorf, Experimentally validated CO2 ejector operation characteristic used in a numerical investigation of ejector cycle, Int. J. Refrig. 36 (2013) 881–891.

[16] Z. Bilicki, J. Kestin, Physical aspects of the relaxation model in two-phase flow, Proceedings of the Royal Society of London A: Mathematical, Physical and Engineering Sciences 428 (1875) (1990) 379–397.

[17] A. Attou, J. Seynhaeve, Steady-state critical two-phase flashing flow with possible multiple choking phenomenon part 1: physical modelling and numerical procedure, J. Loss Prev. Process Ind. 12 (1999) 347–359 September.

[18] W. Angielczyk, Y. Bartosiewicz, D. Butrymowicz, J.-M. Seynhaeve, 1-D modeling of supersonic carbon dioxide two-phase flow through ejector motive nozzle, International Refrigeration and Air Conditioning Conference, Purdue, USA, (2010).

[19] M.D. Lorenzo, P. Lafon, J.-M. Seynhaeve, Y. Bartosiewicz, Benchmark of delayed equilibrium model (DEM) and classic two-phase critical flow models against experimental data, Int. J. Multiph. Flow 92 (2017) 112–130.

[20] Y. Bartosiewicz, M. Giot, J.-M. Seynhaeve, Revisiting Modeling Techniques and Validation Experiments for Twophase Choked flows Relevant to Loca. The 8th International Topical Meeting on Nuclear Thermal-hydraulics, Operation and Safety (NUTHOS-8) N8P0317, Shanghai, 2010.

[21] J.-M. Seynhaeve, A. De Crécy, Y. Bartosiewicz, Uncertainty Analysis of Delayed Equilibrium Model (DEM) Using the Circe Methodology. NURETH-16, Chicago, IL, August 30-September 4, (2015).

[22] R. Span, W. Wagner, A new equation of state for carbon dioxide covering the fluid region from the triple-point temperature to 1100 K at pressures up to 800 MPa, J. Phys. Chem. Ref. Data 25 (6) (1996) 1509–1596.

[23] Z. Bilicki, C. Dafermos, J. Kestin, G. Majda, D. Zeng, Trajectories and singular points in steady-state models of two-phase flows, Int. J. Multiph. Flow 13 (4) (1987) 511–533.

[24] W.H. Press, S.A. Teukolsky, W.T. Vetterling, B.P. Flannery, 3rd ed., Numerical Recipes in C+ +: The Art of Scientific Computing vol. 1002, Cambridge University Press, 2002.

[25] H. De Sterck, Critical point analysis of transonic flow profiles with heat conduction, SIAM J. Appl. Dyn. Syst. 6 (3) (2009) 645–662 2007.

[26] J. Boure, A. Fritte, M. Giot, M. Reocreux, Highlights of two-phase critical flow: on the links between maximum flow rates, sonic velocities, propagation and transfer phenomena in single and two-phase flows, Int. J. Multiph. Flow 3 (1) (1976) 1–22.

[27] V. Feburie, M. Giot, S. Granger, J. Seynhaeve, A model for choked flow through cracks with inlet subcooling, Int. J. Multiph. Flow 19 (4) (1993) 541–562.

[28] L. Bolle, P. Downar-Zapolski, J. Franco, J. Seynhaeve, Experimental and theoretical analysis of flashing water flow through a safety value, J. Hazard. Mater. 46 (2) (1996) 105–116 Heat and Mass Transfer in Chemical Process Industry Accidents.

[29] P. Downar-Zapolski, Z. Bilicki, L. Bolle, J. Franco, The nonequilibrium relaxation model for one-dimensional flashing liquid flow, Int. J. Multiph. Flow 22 (3) (1996) 473–483.

[30] M. Nakagawa, M.S. Berana, A. Kishine, Supersonic two-phase flow of CO2 through converging–diverging nozzles for the ejector refrigeration cycle, Int. J. Refrig. 32 (6) (2009) 1195–1202.

[31] F. Aakenes, S.T. Munkejord, M. Drescher, Frictional pressure drop for two-phase flow of carbon dioxide in a tube: comparison between models and experimental data. Energy procedia, 51:373 – 381, 7th Trondheim Conference on CO2 Capture, Transport and Storage, (2014).

[32] J. Smolka, Z. Bulinski, A. Fic, A.J. Nowak, K. Banasiak, A. Hafner, A computational model of a transcritical r744 ejector based on a homogeneous real fluid approach, Appl. Math. Model. 37 (3) (2013) 1208–1224.

[33] M. Palacz, J. Smolka, A. Fic, Z. Bulinski, A.J. Nowak, K. Banasiak, A. Hafner, Application range of the hem approach for co2 expansion inside two-phase ejectors for supermarket refrigeration systems, Int. J. Refrig. 59 (2015) 251–258.